\$50 WILLIAMS

Contents lists available at ScienceDirect

Earth and Planetary Science Letters

www.elsevier.com/locate/epsl



Inter-relationship and environmental significance of stalagmite δ^{13} C and δ^{18} O records from Zhenzhu Cave, north China, over the last 130 ka



Yunxia Li^{a,b}, Zhiguo Rao^{a,b,*}, Qinghai Xu^c, Shengrui Zhang^c, Xiaokang Liu^b, Zongli Wang^b, Hai Cheng^{d,e}, R. Lawrence Edwards^{e,f}, Fahu Chen^{b,g}

- ^a College of Resources and Environmental Sciences, Hunan Normal University, Changsha 410081, China
- b Key Laboratory of Western China's Environmental Systems (Ministry of Education), College of Earth and Environmental Sciences, Lanzhou University, Lanzhou 73000, China
- ^c College of Resources and Environment, Hebei Key Laboratory of Environmental Change and Ecological Construction, Hebei Normal University, Shijiazhuang 050024, China
- ^d Institute of Global Environmental Change, Xi'an Jiaotong University, Xi'an 710049, China
- ^e Department of Earth Sciences, University of Minnesota, Minneapolis, MN 55455, USA
- f School of Geography, Nanjing Normal University, Nanjing, 210023, China
- ^g Key Laboratory of Alpine Ecology, CAS Center for Excellence in Tibetan Plateau Earth Sciences, Institute of Tibetan Plateau Research, Chinese Academy of Sciences, Beijing 100101, China

ARTICLE INFO

Article history:
Received 8 April 2019
Received in revised form 6 February 2020
Accepted 11 February 2020
Available online 18 February 2020
Editor: L. Robinson

Keywords: stalagmite δ^{18} O δ^{13} C past 130 ka north China EASM

ABSTRACT

There is a vigorous and ongoing debate about the interpretation of the stalagmite δ^{18} O record from east China as an indicator of East Asian summer monsoon (EASM) intensity. This is mainly because of the inconsistent spatial variation of precipitation amount in east China, but the generally consistent variation of precipitation δ^{18} O, on various timescales. However, a direct comparison of a proxy record of precipitation amount with the δ^{18} O record from the same stalagmite has rarely been reported, especially in north China. Here, we present precisely-dated high-resolution stalagmite δ^{13} C and δ^{18} O records for the past 130 ka (1 ka = 1000 years) from Zhenzhu (ZZ) Cave in north China. On multi-millennial to orbital timescales, the δ^{13} C and δ^{18} O records exhibit a high degree of in-phase co-variation; however, there are differences in the trend and amplitude of change between various marine isotopic stages (MIS): specifically, MIS5e, MIS5c, MIS5a, MIS3 and MIS1. Modern monitoring results of two years from ZZ Cave, together with a comparison of the δ^{13} C record from the cave with a pedogenic carbonate δ^{13} C record from the western Chinese Loess Plateau (CLP), demonstrate that the δ^{13} C record is a sensitive and reliable indicator of EASM rainfall amount. Considering that variations in both the amount and δ^{18} O of precipitation can be modulated by the atmospheric circulation system, we conclude that the amplitude and trend of the stalagmite δ^{18} O variations from north China are not an absolute indicator of EASM intensity, but rather an indicator of changes in the phase of the EASM. We suggest that stalagmite δ^{18} O records combined with other unambiguous proxy indicators from stalagmites can provide a more comprehensive history of changes of the EASM.

© 2020 Elsevier B.V. All rights reserved.

1. Introduction

Records of the oxygen isotopic composition (δ^{18} O) of stalagmites from monsoonal China have been intensively studied since the late 1980s (e.g. Zhu et al., 1988). The evolution of the climatic interpretation of these records can be roughly divided into three stages: (i) From the early 1990s, stalagmite δ^{18} O records were

E-mail address: raozhg@hunnu.edu.cn (Z. Rao).

widely proposed as an indicator of temperature (e.g. Li, 1994). (ii) With the publication of the stalagmite δ^{18} O record from Hulu Cave, in the lower reaches of the Yangtze River in central China (Wang et al., 2001; Fig. 1), such records were widely reported as an indicator of the Asian summer monsoon intensity, or monsoonal rainfall amount (e.g. Dong et al., 2015; Cheng et al., 2016). (iii) In recent years, the significance of the stalagmite δ^{18} O record as an indicator of Asian summer monsoon intensity has been increasingly debated (e.g. Pausata et al., 2011; Tan, 2014).

The spatially variable pattern of precipitation amount in east China is well known (Ding et al., 2008), as demonstrated by the instrumentally-observed trend of decreasing summer (June-

^{*} Corresponding author at: College of Resources and Environmental Sciences, Hunan Normal University, Changsha 410081, China.

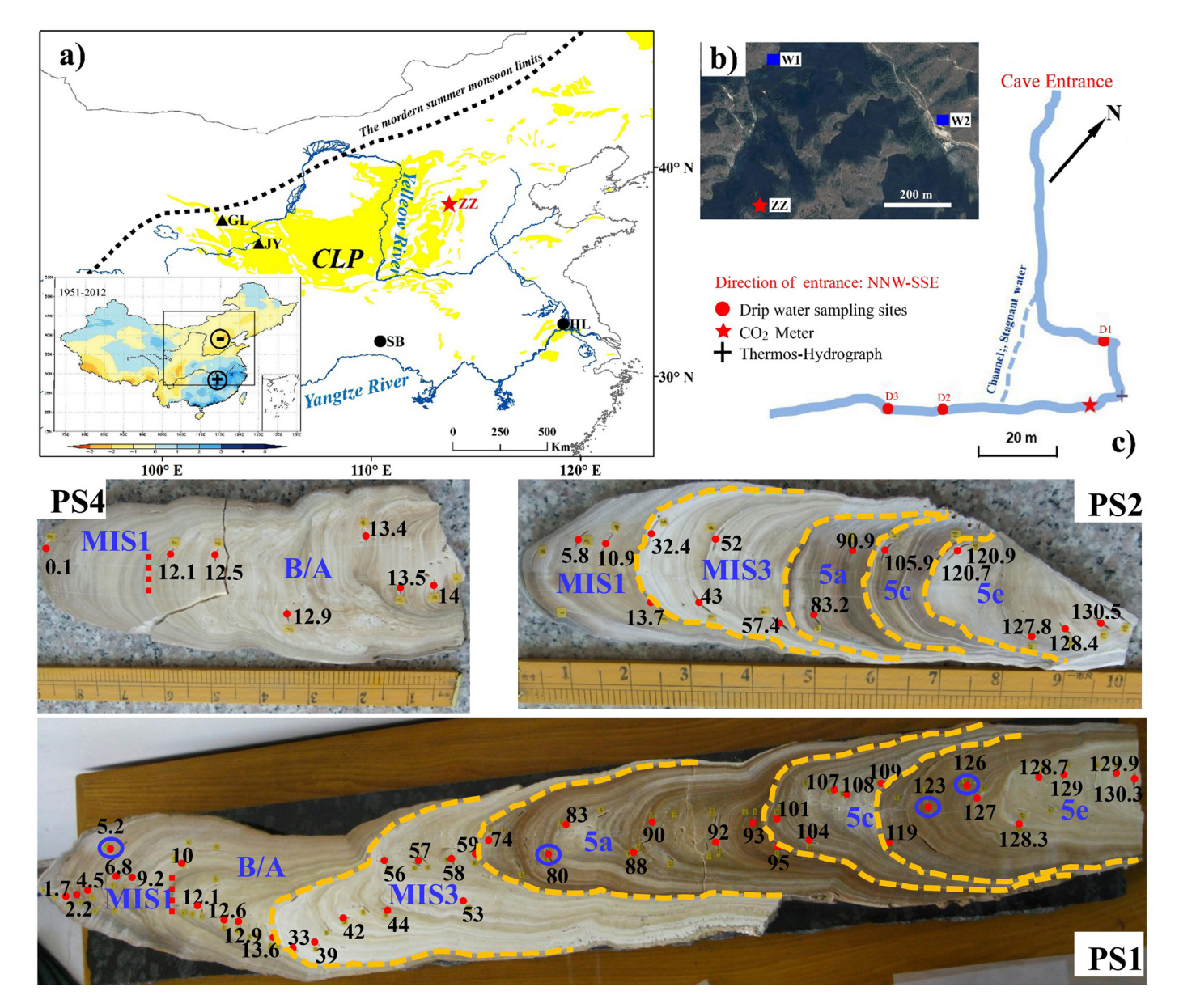


Fig. 1. a) Map showing the locations of ZZ (Zhenzhu) Cave, HL (Hulu) Cave, SB (Sanbao) Cave, and the JY (Jingyuan) and GL (Gulang) loess profiles. The inset panel in the lower-left corner illustrates decreasing and increasing trends of summer precipitation in north China and in central and south China (Liu et al., 2015) over the period of 1951-2012. b) Modern precipitation δ^{18} O monitoring sites outside ZZ Cave (W1 and W2; Li et al., 2019). c) Locations of modern monitoring sites in ZZ Cave (Li et al., 2019). Photos of stalagmite samples PS1, PS2 and PS4 are shown in the lower part, together with the results of ϵ^{230} Th dating (red dots and black Arabic numerals, ka) and the corresponding marine isotopic stages (MIS; bold blue). Bold dashed yellow lines represent depositional hiatuses corresponding to MIS5d, MIS4 and MIS2 in samples PS1 and PS2. The four blue open circles indicate the locations of the dates in sample PS1, with large uncertainties. (For interpretation of the colors in the figure(s), the reader is referred to the web version of this article.)

July-August) precipitation in north China, and the increasing trend in central and south China, during 1951-2012 (Liu et al., 2015; Fig. 1). Consequently, the spatially variable pattern of precipitation amount, together with the generally consistent pattern of variation of precipitation δ^{18} O in east China on various timescales, has been regarded as important evidence challenging the significance of the stalagmite δ^{18} O record as an indicator of East Asian summer monsoon (EASM) intensity. Three examples are summarized as follows: (i) For the past \sim 1000 years, a synthesis of paleoclimatic results (Chen et al., 2015) has demonstrated the pattern of a relatively humid/arid north/south China during the Medieval Warm Period (MWP), and the opposite pattern during the Little Ice Age (LIA). Notably, however, stalagmite δ^{18} O data from both south and north China were generally more negative/positive during the MWP/LIA (Yang et al., 2014). (ii) Studies of Holocene paleo-humidity in China demonstrate a roughly opposite pattern of variation in north and central China (Rao et al., 2016a), and a "-+-" pattern (i.e. less rainfall in north China, more rainfall in central China, and less rainfall in south China) for the early and late Holocene, and a corresponding "+-+" pattern for the mid-Holocene for south, central and north China (Rao et al., 2016b); however, Holocene stalagmite δ^{18} O records from south, central and north China show similar long-term positive trends (Rao et al., 2016a; 2016b). (iii) For the abrupt climatic events during the last deglaciation, results from the middle Yangtze region indicate a wet Younger Dryas (YD) interval and a dry Bølling-Allerød (B/A) interval, which is the opposite to the pattern in north China (Zhang et al., 2018). However, stalagmite δ^{18} O data from both the middle Yangtze region and north China are less negative during the YD and more negative during the B/A interval (Dong et al., 2015).

Three points can be made regarding the foregoing observations. First, the paleo-humidity results used for comparison with stalag-

mite δ^{18} O records are mainly from loess (e.g. Lu et al., 2013; Rao et al., 2015), lake (e.g. Rao et al., 2016a; 2016b) and peat sediments (e.g. Xie et al., 2013; Zhang et al., 2018), which may lead to uncertainties due to differences in the quality of the chronology from these different sediment types. At present, paleo-humidity results that are directly derived from stalagmites, and indicated by a magnetic parameter (Xie et al., 2013) and elemental ratios (Zhang et al., 2018), are mainly from the middle Yangtze region in central China, and are rarely reported from other regions, especially north China. However, precipitation δ^{18} O data from north China have been suggested to be closely related to precipitation amount (Liu et al., 2014). Second, an enhanced EASM will penetrate further northward and consequently result in more precipitation in north China, and therefore precipitation amount in north China has been proposed as a more reliable indicator of EASM intensity (e.g. Liu et al., 2015). Third, in contrast with many published stalagmite records from south-central China, there are only a few reported stalagmite records for north China, especially records spanning glacial/interglacial cycles. All of the foregoing factors emphasize the need for stalagmite-related proxy records spanning glacial/interglacial cycles from north China.

Here we report stalagmite $\delta^{13}\text{C}/\delta^{18}\text{O}$ records spanning the past 130 ka from Zhenzhu Cave (Fig. 1) in north China. The $\delta^{13}\text{C}$ record has been determined to be a sensitive indicator of local precipitation amount, and therefore a reliable indicator of EASM intensity. Consequently, comparison of the $\delta^{13}\text{C}$ and $\delta^{18}\text{O}$ records enables us to evaluate the relationship between stalagmite $\delta^{18}\text{O}$ and EASM intensity in north China.

2. Materials and methods

2.1. Zhenzhu Cave

Zhenzhu Cave (ZZ; 38.26°N, 113.72°E, \sim 974 m a.s.l.) is small (\sim 100 m in length), with a small entrance and a very narrow passage, located on the top of Tiangui Mountain in Pingshan County, Hebei Province, in temperate north China (Fig. 1). It is located on the eastern flank of the Taihang Mountains, as well as on the eastern edge of the Chinese Loess Plateau (CLP, Fig. 1). It has a NNW-SSE orientation and there is a very thin (\sim 10 m) overlying layer of upper Cambrian - lower Ordovician dolomite, lime-dolomite and dolomitic limestone (Yin et al., 2017). The modern natural vegetation of the area, including above ZZ Cave, is well developed and dominated by temperate broadleaved deciduous forest.

The modern climate of the study area is dominated by the East Asian monsoon system, characterized by warm/humid summers and cold/dry winters. Instrumental data (1981–2010) from the nearest meteorological station in Pingshan city indicate a mean annual temperature (MAT) of $\sim\!13\,^{\circ}\text{C}$ and mean annual precipitation (MAP) of $\sim\!540$ mm, with $\sim\!80\%$ of the MAP occurring in summer (June-September). Due to the higher elevation of ZZ Cave, the MAT at the site ($\sim\!8\text{-}11\,^{\circ}\text{C}$) is $\sim\!2\text{-}3\,^{\circ}\text{C}$ lower, and the MAP ($\sim\!650\text{-}690$ mm) $\sim\!110$ mm higher, than the values in Pingshan city. In situ monitoring results demonstrate that the relative humidity and temperature in ZZ Cave were 99–100% and 9±1°C, respectively, during April 2012 to April 2014 (Li et al., 2019). The stable internal temperature (which is consistent with the outside MAT) and relative humidity clearly indicate that the internal environment of ZZ Cave is relatively closed.

2.2. Stalagmite samples and analytical methods

In 2008, we collected three stalagmite samples from the deep inner part of ZZ Cave. The samples were labeled PS1, PS2 and PS4 and have lengths of \sim 122.3, \sim 30 and \sim 27 cm, respectively (Fig. 1). After transport to the laboratory, the stalagmites were cleaned and

then cut longitudinally along the growth axis using a table-type cutting saw. The face of the cut \sim 4-cm-thick stalagmite was then polished using a FLEX hand-held polisher.

Sub-samples (\sim 100 mg) for 230 Th dating were collected from the cleaned stalagmite profile. All of the sub-samples for dating were obtained from along the growth layers, close to the stalagmite axis, using a hand-held drill, and were placed in 2-ml beakers. Following chemical pretreatment methods described previously (e.g. Cheng et al., 2013), uranium and thorium ions were separated and extracted in a cleanroom laboratory and were then redissolved. The sample solutions were sent to a MC-ICP-MS (Multi-Collector Inductively Coupled Plasma Mass Spectrometer) for ion testing and abundance measurements. Chemical pre-processing of the sub-samples was performed in a clean room and the uranium and thorium detection experiments were run on a Thermo-Fisher Neptune at the Department of Earth Sciences, University of Minnesota, from November 2010 to February 2011. Finally, 54, 15 and 7 230Th ages were obtained for PS1, PS2 and PS4, respectively (Fig. 1).

The longest PS1 was selected for detailed analyses of $\delta^{13}C/\delta^{18}O$. Stalagmite PS2 was also selected for $\delta^{13}C/\delta^{18}O$ analyses, for comparison with the data from PS1. Therefore, some 2400/550 samples were collected from along the growth axis of PS1/PS2 at a resolution of \sim 0.5 mm per sample. The measurements were made on a Thermo/Finnigan mass spectrometer (MAT253) equipped with a Kiel IV Carbonate Device at the Key Laboratory of Western China's Environmental Systems (Ministry of Education), Lanzhou University. International standard materials (GBW04405, GBW04406, NBS18 and NBS19) were run every 20 samples to check for the homogeneity and reproducibility of the results. The results showed that the precision of $\delta^{18}O/\delta^{13}C$ analysis is better than 0.05%/0.03% (2σ , VPDB).

2.3. Modern monitoring

In order to provide a basis for the interpretation of the ZZ δ^{13} C/ δ^{18} O records, a two-year monitoring program from April 2012 to April 2014 was conducted. Precipitation samples at two sites near ZZ Cave, and dripwater samples from three locations inside ZZ Cave (Fig. 1), were collected monthly for δ^{18} O measurements. The CO₂ concentration of the cave air was measured monthly with a CO₂ meter at the same location (Fig. 1). A thermohygrograph was emplaced inside the cave (Fig. 1) to monitor internal air temperature and relative humidity (average hourly output). The detailed results were reported previously (Li et al., 2019).

3. Results

3.1. Modern monitoring results from ZZ Cave

During the two-year monitoring program, the monthly mean atmospheric temperature (MMT) from a climate station at Shijiazhuang (~80 km from ZZ Cave) varied seasonally with a range of \sim 33°C and a mean of \sim 14.4°C. The monthly precipitation amount (MP) from Shijiazhuang station was higher/lower during summer/winter, with distinct seasonal changes (Fig. 2). In contrast, both the air temperature (Tin) and relative humidity (RH) inside ZZ Cave were roughly constant, with a MMT of \sim 9 °C, with a standard deviation of 1 °C, and with the relative humidity varying from \sim 99–100% (Fig. 2), demonstrating the stable conditions inside ZZ Cave. Over the monitoring period, the precipitation $\delta^{18}\mathrm{O}$ data from two outside sites showed similar seasonal variations, ranging from $\sim -4\%$ to $\sim -12\%$, with the values generally more negative/positive in summer/winter. However, the dripwater δ^{18} O data from the three inside sites were almost constant around the mean value of $\sim 9.1\%$; thus a seasonal signal is absent (Fig. 2), implying the

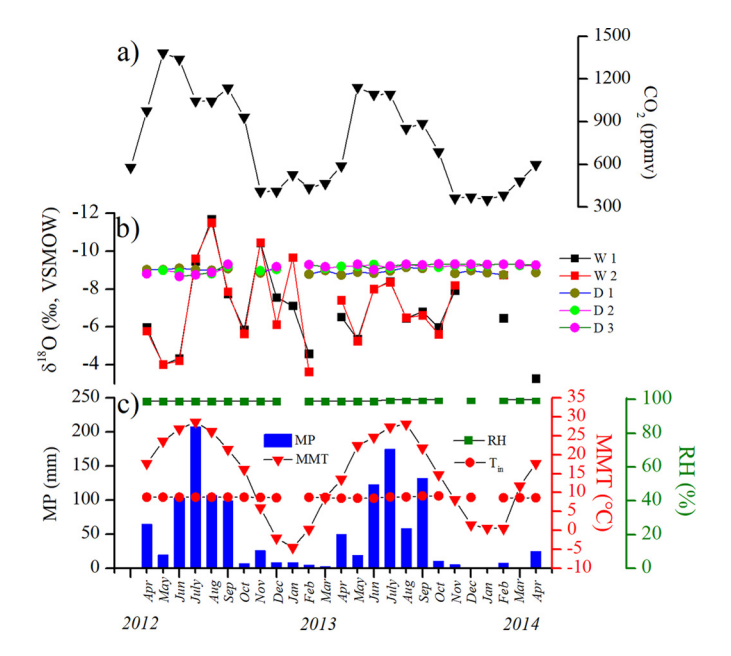


Fig. 2. Results of the two-year modern monitoring of ZZ Cave. (a), air CO $_2$ concentration in the cave; (b) δ^{18} O values of dripwater at three sites inside the cave and precipitation at two sites outside the cave; (c) relative humidity and temperature in the cave and monthly precipitation amount and monthly mean temperature at Shijiazhuang (Li et al., 2019).

"buffer effect" on the groundwater. Notably, the air CO_2 concentration in ZZ cave exhibited clear seasonal variations, with values during summer of ~ 900 to ~ 1300 ppmv, which are two to three times higher than the values of ~ 350 to ~ 400 ppmv during winter (Li et al., 2019; Fig. 2).

3.2. Chronology of the stalagmite samples

U-Th isotopic compositions of the 76 samples, together with the ²³⁰Th dates with 2-sigma uncertainties, are listed in Supplementary Table S1. All of the 7 and 15 dates from PS4 and PS2, respectively, are shown in Fig. 1, as well as some of the 54 dates from PS1. Although a few of the dates from PS1 have unacceptably large uncertainties, as indicated by the blue open circles in both Fig. 1 and Fig. 3, notably these dates are located in the darkcolored 'dirty' parts of PS1 (Fig. 1), indicating more detrital material inputs, as is demonstrated by the corresponding anomalously higher ²³²Th concentrations (Supplementary Table S1). However, all of the PS1 dates are in stratigraphic order (Fig. 3; Supplementary Table S1). Although the lengths of PS4 and PS2 (\sim 27 and \sim 30 cm) are similar, the dates indicate that they were developed during the past \sim 14 and \sim 130 ka, respectively. In addition, although the lengths of PS2 and PS1 (\sim 30 and \sim 122.3 cm) are substantially different, both of them were developed during the past \sim 130 ka (Fig. 1). Thus it appears that there are markedly different growth rates among different ZZ stalagmites.

According to the 230 Th chronologies, there are four sedimentation hiatuses in both PS2 and PS1, roughly corresponding to marine isotopic stage (MIS) 2, MIS4, MIS5b and MIS5d (Fig. 1). More specifically, the four hiatuses in PS1 are within the intervals of \sim 98–97, \sim 87–86, \sim 57–56 and \sim 31–30 cm, with the corresponding age intervals of \sim 119–109 (\sim MIS5d), \sim 101–95 (\sim MIS5b), \sim 74–59 (\sim MIS4) and \sim 33–14 ka (\sim MIS2) (Fig. 1; Supplementary Table S1). Based on this evidence, we regard the 230 Th chronology of PS1 as reliable and we established the resulting age model based on linear interpolation and extrapolation of adjacent 230 Th ages, as shown in Fig. 3. In addition, the age model generated using StalAge method (Scholz and Hoffmann, 2011) is broadly consistent

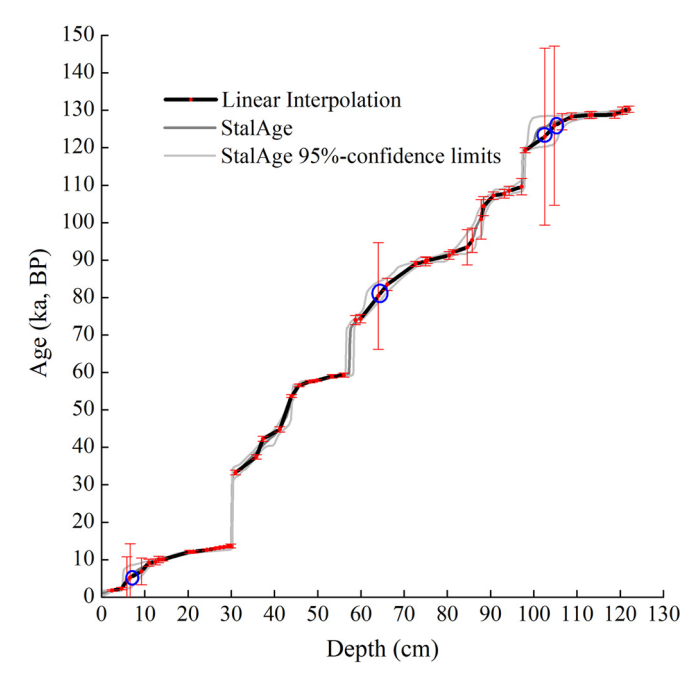


Fig. 3. Age-depth models for stalagmite sample PS1 derived from linear and StalAge (Scholz and Hoffmann, 2011) methods. The four blue open circles indicate dates with large uncertainties (the same as in Fig. 1).

with the linear age model (Fig. 3); therefore the latter was adopted in the final results.

3.3. δ^{18} O and δ^{13} C records from stalagmite PS1

A total of 2364 pairs of δ^{13} C/ δ^{18} O data from the 2391 PS1 samples were obtained. Only 27 samples failed to provide reliable data, mainly because there was insufficient material for isotopic analysis. If the hiatuses are taken into account, the average age resolution of the PS1 δ^{13} C/ δ^{18} O records is \sim 34 years per sample (Supplementary Table S2). The PS1 δ^{18} O values vary from -10.8% to -6.5%, with an average of -9.2% and a range of $\sim 4.3\%$. The PS1 δ^{13} C values vary from -9.4% to -2.9%, with an average of -6.3%and a range of \sim 6.5‰. In general, the absolute PS1 δ^{13} C values are more positive than the PS1 δ^{18} O values, and the range of δ^{13} C values is greater than the range of δ^{18} O values (Supplementary Table S2). In addition, a total of 546 pairs of δ^{13} C/ $\delta^{\hat{18}}$ O data from PS2 represent an average time resolution of \sim 120 years per sample (Supplementary Table S3), a much lower time resolution relative to the data from PS1. However, despite the fewer dates for PS2 (15 vs. 54) and therefore larger uncertainties in the PS2 chronology and the much lower time resolution of the PS2 δ^{13} C/ δ^{18} O data (\sim 120 vs. \sim 34 years per sample), the PS2 δ^{13} C/ δ^{18} O records are highly consistent with those from PS1, especially on the orbital timescale (Supplementary Fig. S1). This highlights the reliability of the δ^{13} C/ δ^{18} O records from PS2/PS1. We therefore chose the PS1 $\delta^{13}\text{C}/\delta^{18}\text{O}$ records for the further analyses and discussion.

As demonstrated by the correlative negative/positive δ^{18} O excursions, especially on the orbital timescale as indicated by the gray bars in Figs. 4a and 4b, during the past 130 ka, the PS1 δ^{18} O record from north China (Fig. 4b) substantially resembles the composite δ^{18} O record (Fig. 4a) from Sanbao (SB) and Hulu (HL) caves (Fig. 1) in the middle and lower reaches of the Yangtze River, respectively, in central China (Wang et al., 2001; 2008). Notably, in the SB/HL δ^{18} O record, the generally more negative δ^{18} O values of \sim 11% to \sim 10% during MIS5e, MIS5c, MIS5a, MIS3 and MIS1 show minimal differences, as is also the case for the PS1 δ^{18} O record (Figs. 4a and 4b). This differs from the record of North Hemisphere summer insolation (NHSI) which shows a long-term

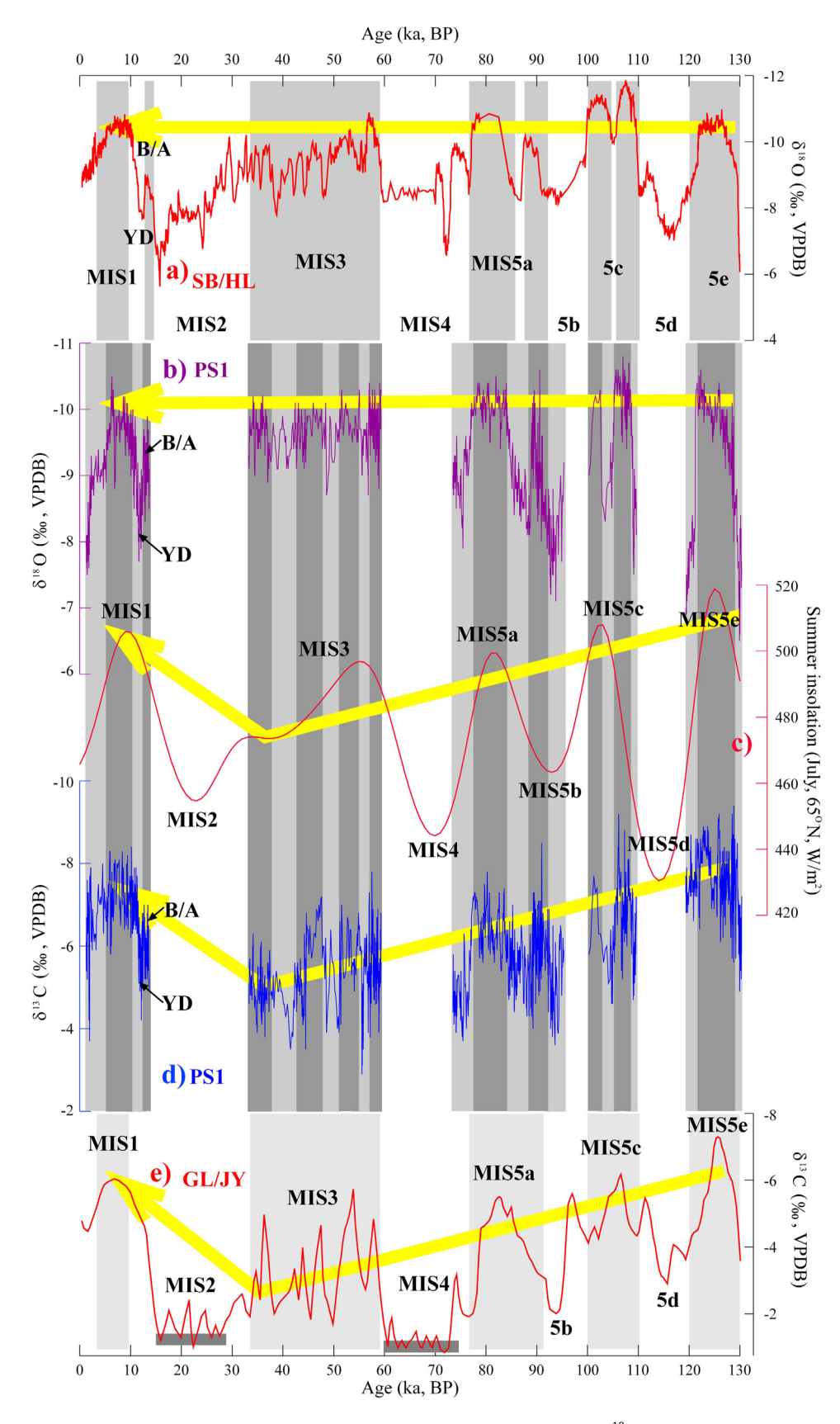


Fig. 4. Comparison of relevant paleoenvironmental records over the past 130 ka, including the SB/HL stalagmite δ^{18} O records from central China (a, Wang et al., 2008), the PS1 δ^{18} O record from north China (b, this study), NHSI (c, average values for July at 65°N; Laskar et al., 2004), the PS1 δ^{13} C record from north China (d, this study), the JY/GL pedogenic carbonate δ^{13} C record from the western edge of the CLP in north China (e, Sun et al., 2015). The negative and positive excursions evident in the δ^{18} O and δ^{13} C records are indicated by the dark-gray and light-gray vertical bars. Long-term trends in these records among MIS5e, MIS5a, MIS3 and MIS1 are indicated by the yellow arrows.

decreasing trend from MIS5e to MIS5c to MIS5a to MIS3, and then an increasing trend to MIS1 (Fig. 4c).

As demonstrated by the correlative negative/positive δ^{13} C excursions, especially on the orbital timescale (Figs. 4d and 4e) during the past 130 ka, the PS1 δ^{13} C record from ZZ Cave (Fig. 4d) on the eastern edge of the CLP (Fig. 1), closely resembles the pedogenic carbonate δ^{13} C record (Fig. 4e) from the JY/GL (Jingyuan/Gulang) loess profiles (Fig. 1) on the western edge of the CLP (Sun et al., 2015). This is despite the fact that the resolution of the JY/GL δ^{13} C record is lower, and the quality of the independent opticallystimulated luminescence chronology of the JY/GL δ^{13} C record is relatively poor. On the orbital timescale, both the PS1 and JY/GL δ^{13} C records show long-term positive trends from MIS5e to MIS5c to MIS5a to MIS3, and subsequently more negative trends to MIS1 (Figs. 4d and 4e), implying a greater similarity with NHSI (Fig. 4c) compared to the PS1 δ^{18} O record.

In summary, the PS1 δ^{13} C/ δ^{18} O time series exhibit two major attributes. First, the δ^{13} C/ δ^{18} O records show a high degree of in-phase co-variation on multi-millennial to orbital timescales, as demonstrated by the 11 negative excursions during \sim 128.8–121.2, \sim 108.7–105.2. \sim 102.8–101.2. \sim 91.0–88.9. \sim 84.2–77.0. \sim 59.3–56.9. \sim 55.1–50.9, \sim 48.4–42.0, \sim 36.9–33.5, \sim 13.5–12.5 and \sim 11.4–5.5 ka in the $\delta^{18}O/\delta^{13}C$ records (Figs. 4b-d), and by the 12 positive excursions during \sim 130.3–128.8, \sim 121.2–119.3, \sim 109.6–108.7, \sim 105.2-102.8, \sim 95.3-91.0, \sim 88.9-84.2, \sim 77.0-74.0, \sim 56.9-55.1, \sim 50.9-48.4, \sim 42.0-36.9, \sim 12.5-11.4 ka, and since \sim 5.5 ka, in the $\delta^{18}O/\delta^{13}C$ records (Figs. 4b-d). During the well-documented abrupt climatic events of the YD and B/A, both the PS1 δ^{18} O/ δ^{13} C values are relatively more positive/negative, respectively (Figs. 4b, 4d), supporting the in-phase co-variation of the PS1 δ^{18} O/ δ^{13} C records. Second, the trends and amplitudes of variation of the PS1 $\delta^{18} \text{O}/\delta^{13} \text{C}$ records corresponding to MIS5e, MIS5c, MIS5a, MIS3 and MIS1 are different. Specifically, during intervals of MIS5e, MIS5c, MIS5a, MIS3 and MIS1 with higher NHSI, the PS1 δ^{18} O values are generally more negative, with the absolute $\delta^{18}O$ values in the range of \sim -10.8\% to \sim -9.5\%, and without apparent differences among them (Fig. 4b). However, the PS1 δ^{13} C data show a longterm positive trend from MIS5e to MIS5c to MIS5a to MIS3, and then a negative trend to MIS1 (Fig. 4d), which is similar to the NHSI (Fig. 4c).

4. Discussion

4.1. Factors controlling the PS1 δ^{13} C record

In principle there are three potential carbon sources for cave stalagmites (e.g. Genty et al., 2001; McDermott, 2004; Breecker, 2017): atmospheric CO₂ (normally with $\delta^{13}C$ values around $-8\%\sim-6\%$), soil plant-root respired CO₂ (normally with $\delta^{13}C$ values more negative than -20%), and bedrock carbonate (CaCO₃ - normally with $\delta^{13}C$ values around 0%). Generally, for caves with overlying vegetation, the high partial pressure of soil plant-root respired CO₂ (pCO₂) will prevent the direct diffusion of atmospheric CO₂ into soil. Therefore, the soil solution with dissolved biogenetic CO₂ will erode the bedrock carbonate, finally forming the seepage solution which enters the cave systems and contains dissolved inorganic carbon (DIC). Consequently, the $\delta^{13}C$ values of DIC ($\delta^{13}C_{\text{DIC}}$) in the seepage solution are mainly controlled by the contribution ratios of biogenetic CO₂ and bedrock carbonate, with more negative/positive $\delta^{13}C$ values (e.g. Fairchild et al., 2006).

The seepage solution $\delta^{13}C_{DIC}$ and the subsequent final stalagmite $\delta^{13}C$ could be further influenced by within-cave processes such as CO_2 degassing and prior calcite precipitation (PCP) (e.g. Fairchild et al., 2006). That is, the lower within-cave pCO_2 will increase the CO_2 degassing from dripwater, resulting in the preferential escape of $^{12}CO_2$ and therefore more positive $\delta^{13}C$ values

of the residual DIC and the stalagmite. Conversely, the PCP process will result in the preferential precipitation of ^{13}C over ^{12}C from seepage solution, and therefore more negative $\delta^{13}\text{C}$ values of the residual DIC (Fairchild et al., 2006). However, due to fact that PCP is also significantly driven by CO₂ degassing, the overall more positive $\delta^{13}\text{C}$ values of the residual DIC and the stalagmite will result from the coupled effect of increased CO₂ degassing and consequently increased PCP.

Within-cave CO_2 degassing mainly depends on the pCO_2 gradient between the dripwater and the cave air, and the cave air CO_2 concentration is mainly controlled by the overlying soil CO_2 and/or cave ventilation. Cave ventilation is normally controlled by the internal-external temperature gradient and the associated air pressure gradient, as well as by the cave morphology and the entrance position/orientation (e.g. Spötl et al., 2005; Tremaine et al., 2011). Specifically, in summer, as cave internal air is colder/denser than the external air, the ventilation effect will be relatively weak which therefore helps trap CO_2 within the cave, increasing the cave pCO_2 and suppressing within-cave CO_2 degassing, finally resulting in more negative $\delta^{13}C$ values of the residual DIC and the stalagmite; and vice versa in winter (e.g. Fairchild et al., 2006).

For ZZ Cave, over the monitoring period, the in situ measured internal pCO₂ increased rapidly in late spring (March-April) and reached peak values in early summer (May-June/July; Fig. 2). Interestingly, during the subsequent month with the greatest externalinternal temperature gradient (July 2012 and August 2013; Fig. 2), the internal pCO₂ was slightly decreased (Fig. 2), implying an insignificant ventilation effect within the cave. More importantly, the other cave parameters could also be strongly influenced by a significant seasonal ventilation effect. For example, in Heshang Cave (in central China) which has an open nature, and Liangfeng Cave (in southwest China) with a potentially significant ventilation effect, apparently seasonal variations in cave temperature, cave humidity, and cave dripwater δ^{18} O have been observed (Hu et al., 2008; Zeng et al., 2015; Duan et al., 2016). Notably, the internal pCO2 of Heshang Cave also shows seasonal variations within the relatively narrow range of ~335-592 ppmv, with higher values in winter (Hu et al., 2008). Thus the apparently seasonal pCO2 variations in ZZ Cave, with higher values in summer (Fig. 2), cannot be regarded as the result of a dominant ventilation effect. In contrast, the almost constant internal temperature, relative humidity and dripwater δ^{18} O of ZZ Cave over the two years of monitoring (Fig. 2) clearly demonstrate that the ventilation effect is not significant in this cave. Thus the large pCO_2 increase, from \sim 350-400 ppmv in winter to \sim 900–1300 ppmv in summer (Li et al., 2019; Fig. 2), should be mainly due to soil root-respired CO2, although the potential (but insignificant) effect of cave ventilation cannot be completely excluded.

We therefore propose the following control mechanisms for the stalagmite δ^{13} C values in ZZ Cave. During the warmer/wetter summer months, enhanced soil root respiration results in more soil CO_2 with more negative $\delta^{13}C$ values, which finally contributes to the more negative $\delta^{13}C$ values of the stalagmite, and vice versa for the winter months. Such seasonal $\delta^{13}C$ differences could be further amplified by other within-cave processes, such as the abovementioned within-cave CO₂ degassing and PCP (Liu et al., 2016). Much higher soil pCO₂ in summer, along with the more negative $\delta^{13}C_{DIC}$ in both soil water and cave dripwater, and with the higher cave pCO_2 and the more negative $\delta^{13}C$ of the cave air CO_2 , have been reported in several caves, such as in Furong Cave in southwest China (Li et al., 2012; Huang et al., 2016) and in Obir Caves in Austria (Spötl et al., 2005). These observations support our proposed control mechanisms. Notably, the ventilation effect has been proposed to be more significant during winter (e.g. Breecker et al., 2012), implying that even if there is insignificant ventilation in ZZ Cave during winter, the above-mentioned seasonal δ^{13} C differences

will be amplified rather than smoothed. Thus our proposed control mechanisms for the stalagmite $\delta^{13}C$ data from ZZ Cave will not be significantly affected by the ventilation effect.

Interestingly, during the summers (June-September) of 2012 and 2013, the average MMT at Shijiazhuang station was \sim 25.7 $^{\circ}$ C and ~ 25.4 °C, respectively; the precipitation amount was ~ 516 mm and ~487 mm, respectively; and the average air CO₂ concentration was \sim 1140 ppmv and \sim 980 ppmv, respectively. Thus it appears that the air CO₂ concentration within ZZ Cave is more closely related to precipitation amount; that is, more negative stalagmite δ^{13} C values can be expected due to more root-respired CO₂ being produced under more humid conditions. Notably, the previouslyreported modern observational results have demonstrated that the dripwater $\delta^{13}C_{DIC}$ variations in Furong Cave in southwest China mainly responded to local precipitation changes and the overlying humidity conditions (Huang et al., 2016), supporting our results from ZZ Cave. Considering the absence of seasonal dripwater δ^{18} O variations but apparently seasonal pCO₂ variations in ZZ Cave (Li et al., 2019; Fig. 2), it appears that the stalagmite δ^{13} C data from ZZ Cave are a potentially more sensitive indicator of climatic changes than stalagmite δ^{18} O data, especially of changes in local precipitation amount. The local precipitation amount at the ZZ site is dominated by the East Asian monsoon system. More importantly, considering that the enhanced EASM will penetrate further northward and result in more monsoonal rainfall in north China (e.g. Liu et al., 2015), we therefore finally conclude that the stalagmite δ^{13} C data from ZZ Cave are an indicator of EASM intensity, with more negative δ^{13} C values corresponding to enhanced EASM intensity, and vice versa.

The Chinese loess pedogenic carbonate δ^{13} C record is mainly determined by the ratio of the two end members of detrital carbonate and the overlying vegetation (Rao et al., 2006), which is similar to the mechanism affecting the ZZ Cave stalagmite δ^{13} C, as mentioned above. Furthermore, in the CLP, loess pedogenic carbonate δ^{13} C data have been proposed as an indicator of vegetation density and therefore as an indirect indicator of local rainfall amount, hence EASM intensity (Rao et al., 2006; Sun et al., 2015). Therefore, the similarity of the controlling mechanisms and the consistency between the PS1 and JY/GL δ^{13} C records over the past 130 ka (Figs. 4d, 4e) further reinforce the utility of the PS1 δ^{13} C record as a sensitive and reliable indicator of EASM intensity.

4.2. Interpretation of the similarity and difference between the PS1 $\delta^{18}{\rm O}$ and $\delta^{13}{\rm C}$ records

It is well-known that stalagmite $\delta^{18}O$ records from monsoonal China are generally spatially consistent on various timescales. This is demonstrated over the past \sim 14.5 ka by the stalagmite δ^{18} O record from Lianhua Cave in north China, which largely replicates the stalagmite δ^{18} O records from low-latitude Chinese monsoonal regions (Dong et al., 2015), and by the consistency between the PS1 and SB/HL δ^{18} O records over the past 130 ka (Figs. 4a, 4b). Therefore, the co-variations of the PS1 δ^{18} O/ δ^{13} C records on multimillennial to orbital timescales (Figs. 4b, 4d) could not have resulted from internal processes within the cave, such as kinetic isotopic fractionation. It has been proposed that repeatable δ^{18} O signals from the same cave and from different caves can be used to evaluate the likelihood of calcite deposition under isotopic equilibrium and the validity of the records for recording environmental changes (e.g. Cheng et al., 2005; Dorale and Liu, 2009). This strongly supports the environmental significance of the covariation of the PS1 δ^{18} O/ δ^{13} C records and confirms that they cannot be the result of within-cave processes.

As above-mentioned, the rainfall amount in north China has been proposed as a more reliable indicator of EASM intensity than in central and south China, since an enhanced EASM will result in more rainfall in north China (Liu et al., 2015). Therefore, the PS1 δ^{13} C record has been proposed as a sensitive indicator of EASM intensity. Notably, the long-term weakening trend of EASM intensity from MIS5e to MIS5c to MIS5a to MIS3, followed by an intensification to MIS1, is reflected by the PS1 δ^{13} C record (Fig. 4d). This pattern is widely supported by the results of paleoclimatic studies of loess from the CLP, especially of MIS5 (e.g. Rao et al., 2015). However, the long-term pattern of EASM variations, in terms of the relative amplitudes of the interstadial/interglacial peaks (MIS5e, MIS5c, MIS5a, MIS3, and MIS1) indicated by the PS1 and JY/GL δ^{13} C records (Figs. 4d, 4e) is less evident in the PS1 and SB/HL δ^{18} O records (Wang et al., 2008); in the latter records, the amplitude of the interstadial/interglacial peaks is relatively constant (Figs. 4a, 4b). Thus the co-variation of the PS1 δ^{18} O/ δ^{13} C records demonstrates a close relationship between the PS1 δ^{18} 0 record and EASM variations; however, the different trends and amplitudes of the variations in the PS1 δ^{18} O/ δ^{13} C records demonstrate that the PS1 δ^{18} O data are not a reliable indicator of absolute changes in EASM intensity.

The paleoclimatic significance of stalagmite $\delta^{18}O$ records from east China has been widely discussed (e.g. Clemens et al., 2010; Pausata et al., 2011). Typically, the stalagmite δ^{18} O record from east China has been linked to EASM intensity via the ratio of summer/winter rainfall amount (e.g. Wang et al., 2001) and to the southward/northward movement of the Intertropical Convergence Zone (ITCZ; Cheng et al., 2005). In addition, a recent study suggested that stalagmite $\delta^{18}O$ in north China is more likely driven by the amount effect than in central and south China (Liu et al., 2014). Other factors, such as winter temperature and different vapor source ratios (Clemens et al., 2010), the upstream "rainout effect" in the Indian monsoonal region (Pausata et al., 2011), and the circulation effect (Tan, 2014), have also been proposed as possible influences on stalagmite δ^{18} O records from east China. Although the proposed factors are different, all of the results emphasize that the stalagmite $\delta^{18}O$ data in monsoonal China, as an indicator of local precipitation δ^{18} O, could be modulated by other factors, in addition to the monsoon system.

Given that EASM variations include two attributes (phase and amplitude), and, based on the PS1 $\delta^{18} \text{O}/\delta^{13} \text{C}$ records from north China (Figs. 4b, 4d), we propose that the stalagmite $\delta^{18} \text{O}$ record from east China is more likely to be an indicator of changes in the phase of the EASM, rather than of changes in its amplitude. For example, in both ZZ and SB/HL caves, the peak $\delta^{18} \text{O}$ values during MIS5c, which are slightly more negative as a whole than those during MIS5e (Figs. 4a, 4b), can be interpreted as indicating an intensified EASM, but they cannot be used to infer that the EASM was stronger during MIS5c than during MIS5e. Essentially, both precipitation amount and precipitation $\delta^{18} \text{O}$ can be synchronously modulated by changes in atmospheric circulation, such as changes in the EASM, and this may be a major cause of the observed covariation of the PS1 $\delta^{18} \text{O}/\delta^{13} \text{C}$ records., but with differences in trends and amplitudes.

The local precipitation δ^{18} O preserved in stalagmite δ^{18} O records from east China is mainly regulated by the monsoon circulation system, especially on the orbital timescale. In addition, as mentioned above, it could potentially be further modulated by other factors. Therefore, we propose the following simplified interpretational model to explain the similarity and difference between the PS1 δ^{18} O/ δ^{13} C records. As demonstrated in Fig. 5, on the orbital timescale, during periods with higher summer insolation, more water vapor with more negative δ^{18} O values will be generated from the warmer tropical ocean surface, which will be transported further inland by the enhanced EASM intensity. This will result in greater monsoonal rainfall amount in north China that recorded by the more negative stalagmite and loess pedogenic carbonate δ^{13} C values; i.e. the PS1 δ^{13} C record could be a more direct indica-

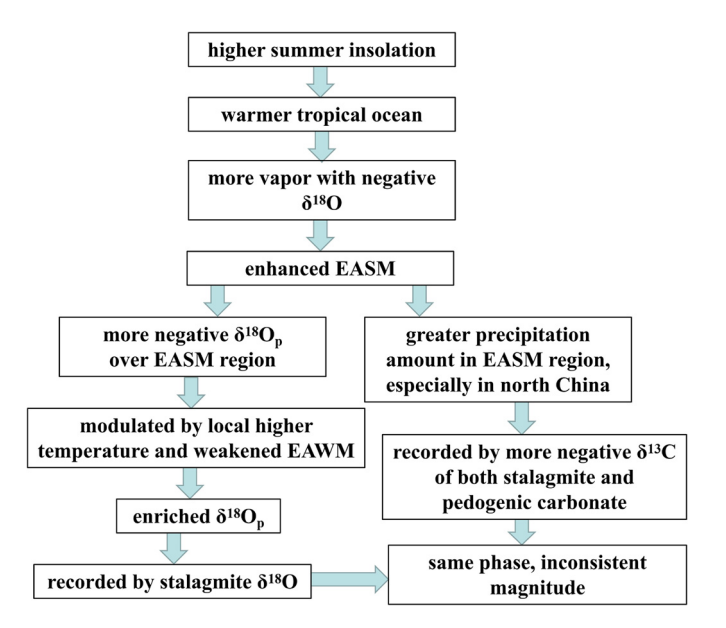


Fig. 5. Proposed simplified interpretational model of the in-phase variations of the PS1 δ^{18} O and δ^{13} C records from north China, with different trends and amplitude of variation, during interstadial/interglacial peaks.

tor of EASM intensity. At the same time, the more negative vapor δ^{18} O over the EASM region could be further affected by other factors. For example, the higher local temperature and the consequent stronger "temperature effect" will result in slightly more positive δ^{18} O values of local precipitation relative to the original water vapor. In addition, the enhanced EASM intensity implies a weaker East Asian winter monsoon and therefore less winter precipitation (normally with more negative δ^{18} O), which could also contribute to the slightly positive δ^{18} O values of local precipitation. That is, the combined positive/negative effects could modulate the local precipitation δ^{18} O values and finally smooth out the differences of the original vapor δ^{18} O values within different interstadial/interglacial peaks with higher NHSI. Consequently, the modulated precipitation δ^{18} O is recorded by the stalagmite δ^{18} O in monsoonal China, finally resulting in the in-phase variations of the PS1 δ^{18} O/ δ^{13} C records from north China, but with different trends and amplitudes of variation, especially during interstadial/interglacial peaks.

4.3. EASM evolution during the past 130 ka

The evolution of EASM intensity over glacial/interglacial cycles and its possible driving mechanisms have been of interest for decades (e.g. Chiang et al., 2015; Cheng et al., 2016; Kong et al., 2017; Clemens et al., 2018). Both earth orbital parameters (eccentricity, obliquity, and precession) and boundary conditions (e.g. global ice volume, greenhouse gas concentration) have been proposed as the dominant factors controlling EASM evolution (e.g. Cheng et al., 2016; Clemens et al., 2018). The operation of these factors is reflected by differences in the dominant cyclicities evident in EASM records reconstructed using different proxies from different geological archives. For example, most loess-based EASM records from north China are characterized by a dominant ~100ka cycle (e.g. Beck et al., 2018), while a dominant \sim 23-ka cycle is present in stalagmite δ^{18} O records in central China (e.g. Cheng et al., 2016). However, possible spatial differences (for example, changes in precipitation amount vary over space, even against the same EASM background; Fig. 1), in addition, the potentially different response of different proxies from different geological archives (e.g. loess and stalagmites) to EASM evolution, limits the direct comparison of records from different archives in different regions. This therefore also limits our understanding of EASM evolution. With their advantages of being derived from the same archive from the same site, and with a common chronology, the PS1 δ^{18} O/ δ^{13} C records from north China, spanning the last 130 ka, provide a major opportunity to provide further insights into the evolution of the EASM and its possible dynamic mechanisms.

To further illustrate their similarity/dissimilarity, and to minimize the effects of differences in the amplitude of the changes, the PS1 δ^{13} C/ δ^{18} O data were normalized to the range of ± 1 and plotted on the same timescale, enabling their direct comparison (Fig. 6a). The PS1 δ^{13} C/ δ^{18} O records exhibit in-phase variations but different long-term trends, especially on the orbital timescale (see yellow arrows in Fig. 6a). Furthermore, to compare the records with those from elsewhere, spectral analysis was conducted on the PS1 δ^{13} C/ δ^{18} O records to identify possible common cyclical components. The REDFIT program in Past3 software, which is an implementation of the REDFIT procedure of Schulz and Mudelsee (2002) was used. As shown in Fig. 6b, the \sim 23-ka cycle is dominant in the PS1 δ^{18} 0 record, which is consistent with stalagmite δ^{18} O records from central China (e.g. Wang et al., 2008). However, the PS1 δ^{13} C record is dominated by the ~100-ka cycle (Fig. 6c). which is consistent with most Chinese loess-based EASM records (e.g. Beck et al., 2018). Notably, with the effects of local temperature and global seawater δ^{18} O removed, a local seawater δ^{18} O record from the Yangtze River Valley, as an indicator of local precipitation and runoff, is dominated by \sim 100-ka and \sim 41-ka cycles, while the \sim 23-ka cycle is absent (Clemens et al., 2018). These results not only support our interpretation of the PS1 δ^{13} C/ δ^{18} O records, but they also imply the potential influence of local temperature on the precipitation δ^{18} O record, as discussed above. All of the above-mentioned results (e.g. Clemens et al., 2018), together with the PS1 δ^{13} C/ δ^{18} O records, highlight the important impacts of boundary conditions (e.g. global ice volume and greenhouse gases) on EASM evolution on the orbital timescale, in addition to insolation. That is, the EASM variations could primarily be triggered by summer insolation and be further modulated by internal forcing mechanisms related to the boundary conditions, as suggested previously (e.g. Sun et al., 2015).

The cessation of the growth of PS1/PS2 during insolation minima (e.g. MIS5d, MIS5b, MIS4 and MIS2: Figs. 1, 3, 4, 6) is a common feature of stalagmites forming in the temperate and frigid zones of the Eurasian continent, such as in caves in semi-arid central Asia (Cheng et al., 2012), the Siberian permafrost zone, the Mongolian Gobi Desert (Vaks et al., 2013), and in the high latitude region of the south central Tibetan Plateau (Cai et al., 2012). It can also be regarded as indicative of an extremely weakened EASM in north China. That is, the hiatuses which occurred in PS1/PS2 during MIS5d, MIS5b, MIS4 and MIS2 could have resulted from the comprehensive effect of extremely decreased EASM intensity, such as: i) the significantly decreased monsoonal rainfall amount due to the southward withdraw of monsoon moisture; ii) the prolonged interval of frozen surface soil overlying the cave; iii) the greatly reduced overlying vegetation cover and the consequent soil CO2 fluxes may have decreased to a level at which percolating groundwater could not reach supersaturation. Notably, during MIS2/MIS4, when the stalagmite growth in ZZ Cave ceased (Fig. 4d), the JY/GL pedogenic carbonate δ^{13} C data are very positive (Fig. 4e), with absolute values of $\sim -2\%$ that close to the $\delta^{13} C$ values of detrital carbonate/carbonate rock, implying the occurrence of severely degraded overlying vegetation conditions during MIS2/MIS4 and therefore to an extremely weakened EASM. Thus an extremely weakened EASM during insolation minima is not in conflict with, but rather is consistent with, the evolution of EASM intensity that is indicated by the PS1 δ^{13} C record: i.e. reduced EASM intensity from MIS5e to MIS5c to MIS5a to MIS3, followed by an intensification to MIS1 (Fig. 6a).

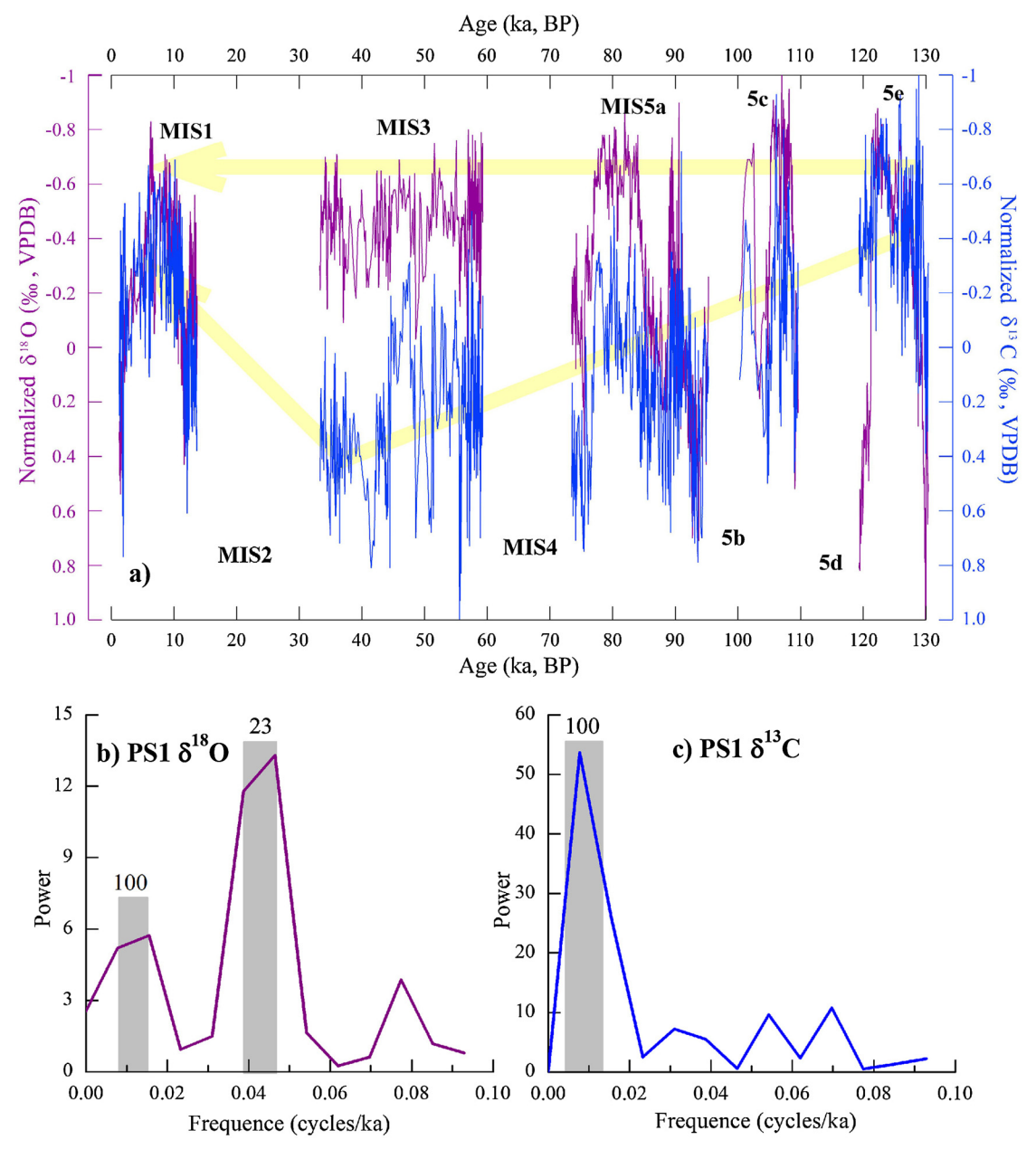


Fig. 6. a) Comparison of the records of normalized PS1 δ^{18} O (purple curve) and δ^{13} C (blue curve) from north China; b) Spectral analysis results of the PS1 δ^{18} O record; c) Spectral analysis results of the PS1 δ^{13} C record.

Finally, although we conclude that the stalagmite δ^{18} O records from monsoonal east China are more likely to be an indicator of EASM phase than absolute EASM amplitude, this does not lessen the importance of Chinese stalagmite $\delta^{18}O$ data for paleoclimatic studies. In other words, stalagmite δ^{18} O records can still be used as an indicator of the phase of the EASM in north, central and south China, due to the observed generally consistent stalagmite δ^{18} O records from these regions on various timescales. This demonstrates the environmental significance of Chinese stalagmite δ^{18} O records, and the fact that they can serve as a benchmark for comparison of paleoclimatic records from different Chinese monsoonal regions. Furthermore, considering the typically high-quality chronologies of stalagmite δ^{18} O records, the changing phases of EASM documented therein can be used to tune other paleoclimatic records from different sediment types. There is little doubt that the combination of stalagmite δ^{18} O records and other paleoclimatic proxy records, including environmental proxies from stalagmites

which have a clear climatic significance, will lead to substantial improvements in our understanding of the past EASM variations.

5. Conclusions

To assess the utility of stalagmite δ^{18} O records as an indicator of the EASM, especially of monsoonal rainfall, we have obtained stalagmite δ^{13} C/ δ^{18} O records spanning the last 130 ka from ZZ Cave in north China. On sub-orbital to millennial timescales, the δ^{13} C and δ^{18} O records co-vary in-phase. However, the δ^{13} C record exhibits a long-term less negative trend from MIS5e to MIS5a to MIS3, followed by a more negative trend to MIS1. This pattern is not evident in the δ^{18} O record from the same stalagmite.

A two-year modern monitoring study of ZZ Cave shows that the $p\text{CO}_2$ in the cave is more sensitive to environmental changes than the dripwater $\delta^{18}\text{O}$ data. Notably, over the past 130 ka, the PS1 $\delta^{13}\text{C}$ record, from the eastern edge of the CLP, exhibits a very sim-

ilar pattern of variation to the δ^{13} C record of pedogenic carbonate from the western edge of the CLP. Based on the similar recording mechanisms of the stalagmite and pedogenic carbonate δ^{13} C signals, the results demonstrate that the PS1 δ^{13} C record is a sensitive and reliable indicator of summer monsoonal rainfall amount.

Given this assumption that summer monsoonal rainfall amount in north China is an indicator of EASM intensity, it is evident that the EASM intensity variations among MIS5e, MIS5c, MIS5a, MIS3 and MIS1, as indicated by the PS1 δ^{13} C record, are not faithfully recorded the PS1 δ^{18} O record. Assuming that both precipitation amount and precipitation δ^{18} O are related to EASM variations, we conclude that the stalagmite δ^{18} O variations in the study region reflect the phase, rather than the intensity, of EASM variations. A more comprehensive understanding of the EASM variations can be obtained by the combined use of δ^{18} O data and other proxy data, with an unambiguous climatic significance, from stalagmites in monsoonal China.

Declaration of competing interest

The authors declare that they have no known competing financial interests or personal relationships that could have appeared to influence the work reported in this paper.

Acknowledgements

This work was supported by the National Natural Science Foundation of China (awards 41772373, 41372181 and 41888101), the Hunan Provincial Natural Science Foundation of China (award 2018JJ1017), the Construction Program for First-Class Disciplines (Geography) of Hunan Province, China, the U.S. NSF (grant 1702816) and the 111 program of China (D19002). We greatly appreciate the valuable and constructive comments of the reviewers. We thank Dr. Jan. Bloemendal for improving the English language.

Appendix A. Supplementary material

Supplementary material related to this article can be found online at https://doi.org/10.1016/j.epsl.2020.116149.

References

- Beck, J.W., Zhou, W.J., Li, C., Wu, Z.K., White, L., Xian, F., Kong, X.H., An, Z.S., 2018. A 550,000-year record of East Asian monsoon rainfall from ¹⁰Be in loess. Science 360, 877–881.
- Breecker, D.O., 2017. Atmospheric pCO₂ control on speleothem stable carbon isotope compositions. Earth Planet. Sci. Lett. 458, 58–68.
- Breecker, D.O., Payne, A.E., Quade, J., Banner, J.L., Ball, C.E., Meyer, K.W., Cowan, B.D., 2012. The sources and sinks of CO₂ in caves under mixed woodland and grassland vegetation. Geochim. Cosmochim. Acta 96, 230–246.
- Cai, Y.J., Zhang, H.W., Cheng, H., An, Z.S., Edwards, R.L., Wang, X.F., Tan, L.C., Liang, F.Y., Wang, J., Kelly, M., 2012. The Holocene Indian monsoon variability over the southern Tibetan Plateau and its teleconnections. Earth Planet. Sci. Lett. 335–336, 135–144.
- Chen, J.H., Chen, F.H., Feng, S., Huang, W., Liu, J.B., Zhou, A.F., 2015. Hydroclimatic changes in China and surroundings during the Medieval Climate Anomaly and Little Ice Age: spatial patterns and possible mechanisms. Quat. Sci. Rev. 107, 98–111.
- Cheng, H., Edwards, R.L., Shen, C.-C., Polyak, V.J., Asmerom, Y., Woodhead, J., Hell-strom, J., Wang, Y.J., Kong, X.G., Spötl, C., Wang, X.F., Alexander Jr., E.C., 2013. Improvements in ²³⁰Th dating, ²³⁰Th and ²³⁴U half-life values, and U-Th isotopic measurements by multi-collector inductively coupled plasma mass spectrometry. Earth Planet. Sci. Lett. 371–372, 82–91.
- Cheng, H., Edwards, R.L., Sinha, A., Spötl, C., Yi, L., Chen, S.T., Kelly, M., Kathayat, G., Wang, X.F., Li, X.L., Kong, X.G., Wang, Y.J., Ning, Y.F., Zhang, H.W., 2016. The Asian monsoon over the past 640,000 years and ice age terminations. Nature 534, 640–646.
- Cheng, H., Edwards, R.L., Wang, X.F., Wang, Y.J., Kong, X.G., Yuan, D.X., Zhang, M.L., Lin, Y.S., Qin, J.M., Ran, J.C., 2005. Oxygen isotope records of stalagmites from southern China. Quat. Sci. 25 (2), 157–163 (in Chinese with English abstract).

- Cheng, H., Zhang, P.Z., Spötl, C., Edwards, R.L., Cai, Y.J., Zhang, D.Z., Sang, W.C., Tan, M., An, Z.S., 2012. The climatic cyclicity in semiarid-arid Central Asia over the past 500,000 years. Geophys. Res. Lett. 39, L01705.
- Chiang, J.C., Fung, I.Y., Wu, C.H., Cai, Y.J., Edman, J.P., Liu, Y.W., Day, J.A., Bhattacharya, T., Mondal, Y., Labrousse, C.A., 2015. Role of seasonal transitions and westerly jets in East Asian paleoclimate. Quat. Sci. Rev. 108, 111–129.
- Clemens, S.C., Holbourn, A., Kubota, Y., Lee, K.E., Liu, Z., Chen, G., Nelson, A., Fox-Kemper, B., 2018. Precession-band variance missing from East Asian monsoon runoff. Nat. Commun. 9, 3364.
- Clemens, S.C., Prell, W.L., Sun, Y.B., 2010. Orbital-scale timing and mechanisms driving late Pleistocene Indo-Asian summer monsoons: reinterpreting cave speleothem δ^{18} O. Paleoceanography 25, PA4207.
- Ding, Y.H., Wang, Z.Y., Sun, Y., 2008. Inter-decadal variation of the summer precipitation in East China and its association with decreasing Asian summer monsoon. Part I: observed evidences. Int. J. Climatol. 28, 1139–1161.
- Dong, J.G., Shen, C.C., Kong, X.G., Wang, H.C., Jiang, X.Y., 2015. Reconciliation of hydroclimate sequences from the Chinese Loess Plateau and low-latitude East Asian Summer Monsoon regions over the past 14,500 years. Palaeogeogr. Palaeoclimatol. Palaeoecol. 435, 127–135.
- Dorale, J.A., Liu, Z.H., 2009. Limitations of Hendy Test criteria in judging the paleoclimatic suitability of speleothems and the need for replication. J. Caves Karst Stud. 71, 73–80.
- Duan, W.H., Ruan, J.Y., Luo, W.J., Li, T.Y., Tian, L.J., Zeng, G.N., Zhang, D.Z., Bai, Y.J., Li, J.L., Tao, T., Zhang, P.Z., Baker, A., Tan, M., 2016. The transfer of seasonal isotopic variability between precipitation and drip water at eight caves in the monsoon regions of China. Geochim. Cosmochim. Acta 183, 250–266.
- Fairchild, I.J., Smith, C.L., Baker, A., Fuller, L., Spötl, C., Mattey, D., McDermott, F., 2006. Modification and preservation of environmental signals in speleothems. Earth-Sci. Rev. 75, 105-153.
- Genty, D., Baker, A., Massault, M., Proctor, C., Gilmour, M., Pons-Branchu, E., Hamelin, B., 2001. Dead carbon in stalagmites: carbonate bedrock paleodissolution vs. ageing of soil organic matter. Implications for ¹³C variations in speleothems. Geochim. Cosmochim. Acta 65, 3443–3457.
- Hu, C.Y., Henderson, G.M., Huang, J.H., Chen, Z.H., Johnson, K.R., 2008. Report of a three-year monitoring programme at Heshang Cave, Central China. Int. J. Speleol. 37, 143–151.
- Huang, C.X., Li, T.Y., Han, L.Y., Li, J.Y., Yuan, N., Wang, H.B., Zhang, T.T., Zhao, X., Zhou, J.L., 2016. Variations of cave water DIC-δ¹³C and its influencing factors in Furong Cave, Chongqing. Carsol. Sin. 36, 299–306 (in Chinese with English abstract).
- Kong, W.W., Swenson, L.M., Chiang, J.C., 2017. Seasonal transitions and the westerly jet in the Holocene East Asian summer monsoon. J. Climate 30, 3343–3365.
- Laskar, J., Robutter, P., Joutel, F., Gastinean, M., Correia, A.C.M., Levrard, B., 2004. A long-term numerical solution for the insolation quantities of the Earth. Astron. Astrophys. 428, 261–285.
- Li, B., 1994. Significance of δ^{13} C, δ^{18} O of speleothems for environmental changes. Carsol. Sin. 13 (1), 17–24 (in Chinese with English abstract).
- Li, T.Y., Li, H.C., Xiang, X.J., Kuo, T.S., Li, J.Y., Zhou, F.L., Chen, H.L., Peng, L.L., 2012. Transportation characteristics of δ^{13} C in the plants-soil-bedrock-cave system in Chongqing karst area. Sci. China Earth Sci. 55, 685–694.
- Li, Y.X., Zhang, S.R., Liu, X.K., Gao, Y.L., Rao, Z.G., 2019. Variations of the stable isotopic composition of precipitation and cave drip water at Zhenzhu Cave, North China: a two-year monitoring study. J. Caves Karst Stud. 81, 123–135.
- Liu, D.B., Wang, Y.J., Cheng, H., Edwards, R.L., Kong, X.G., Li, T.Y., 2016. Strong coupling of centennial-scale changes of Asian monsoon and soil processes derived from stalagmite δ^{18} O and δ^{13} C records, southern China. Quat. Res. 85, 333–346.
- Liu, J.B., Chen, J.H., Zhang, X.J., Li, Y., Rao, Z.G., Chen, F.H., 2015. Holocene East Asian summer monsoon records in northern China and their inconsistency with Chinese stalagmite δ^{18} O records. Earth-Sci. Rev. 148, 194–208.
- Liu, Z.Y., Wen, X.Y., Brady, E.C., Otto-Bliesner, B., Yu, G., Lu, H.Y., Cheng, H., Wang, Y.J., Zheng, W.P., Ding, Y.H., Edwards, R.L., Cheng, J., Liu, W., Yang, H., 2014. Chinese cave records and the East Asia summer monsoon. Quat. Sci. Rev. 83, 115–128.
- Lu, H.Y., Yi, S.W., Liu, Z.Y., Mason, J.A., Jiang, D.B., Cheng, J., Steven, T., Xu, Z.W., Zhang, E.L., Jin, L.Y., Zhang, Z.H., Guo, Z.T., Wang, Y., Otto-Bliesner, B., 2013. Variation of East Asian monsoon precipitation during the past 21 k.y. and potential CO₂ forcing. Geology 41, 1023–1026.
- McDermott, F., 2004. Palaeo-climate reconstruction from stable isotope variations in speleothems: a review. Ouat. Sci. Rev. 23, 901–918.
- Pausata, F.S.R., Battisti, D.S., Nisancioglu, K.H., Bitz, C.M., 2011. Chinese stalagmite δ^{18} O controlled by changes in the Indian monsoon during a simulated Heinrich event. Nat. Geosci. 4, 474–480.
- Rao, Z.G., Jia, G.D., Li, Y.X., Chen, J.H., Xu, Q.H., Chen, F.H., 2016a. Asynchronous evolution of the isotopic composition and amount of precipitation in north China during the Holocene revealed by a record of compound-specific carbon and hydrogen isotopes of long-chain n-alkanes from an alpine lake. Earth Planet. Sci. Lett. 446, 68–76.
- Rao, Z.G., Li, Y.X., Zhang, J.W., Jia, G.D., Chen, F.H., 2016b. Investigating the long-term palaeoclimatic controls on the δD and $\delta^{18}O$ of precipitation during the Holocene in the Indian and East Asian monsoonal regions. Earth-Sci. Rev. 159, 292–305.
- Rao, Z.G., Liu, X.K., Hua, H., Gao, Y.L., Chen, F.H., 2015. Evolving history of the East Asian summer monsoon intensity during the MIS5: inconsistent records from Chinese stalagmites and loess deposits. Environ. Earth Sci. 73, 3937–3950.

- Rao, Z.G., Zhu, Z.Y., Chen, F.H., Zhang, J.W., 2006. Does $\delta^{13}C_{carb}$ of the Chinese loess indicate past C_3/C_4 abundance? A review of research on stable carbon isotopes of the Chinese loess. Quat. Sci. Rev. 25, 2251–2257.
- Scholz, D., Hoffmann, D.L., 2011. StalAge an algorithm designed for construction of speleothem age models. Ouat. Geochronol. 6, 369–382.
- Schulz, M., Mudelsee, M., 2002. REDFIT: estimating red-noise spectra directly from unevenly spaced paleoclimatic time series. Comput. Geosci. 28, 421–426.
- Spötl, C., Fairchild, I.J., Tooth, A., 2005. Cave air control on dripwater geochemistry, Obir Caves (Austria): Implications for speleothem deposition in dynamically ventilated caves. Geochim. Cosmochim. Acta 69, 2451–2468.
- Sun, Y.B., Kutzbach, J., An, Z.S., Clemens, S., Liu, Z.Y., Liu, W.G., Liu, X.D., Shi, Z.G., Zheng, W.P., Liang, L.J., Yan, Y., Li, Y., 2015. Astronomical and glacial forcing of East Asian summer monsoon variability. Quat. Sci. Rev. 115, 132–142.
- Tan, M., 2014. Circulation effect: response of precipitation δ^{18} O to the ENSO cycle in monsoon regions of China. Clim. Dyn. 42, 1067–1077.
- Tremaine, D.M., Froelich, P.N., Wang, Y., 2011. Speleothem calcite farmed in situ: modern calibration of δ^{18} O and δ^{13} C paleoclimate proxies in a continuously monitored natural cave system. Geochim. Cosmochim. Acta 75, 4929–4950.
- Vaks, A., Gutareva, O.S., Breitenbach, S.F.M., Avirmed, E., Mason, A.J., Thomas, A.L., Osinzev, A.V., Kononov, A.M., Henderson, G.M., 2013. Speleothems reveal 500,000-year history of Siberian permafrost. Science 340, 183–186.
- Wang, Y.J., Cheng, H., Edwards, R.L., An, Z.S., Wu, J.Y., Shen, C.C., Dorale, J.A., 2001. A high resolution absolute-dated late Pleistocene monsoon record from Hulu Cave, China. Science 294, 2345–2348.

- Wang, Y.J., Cheng, H., Edwards, R.L., Kong, X.G., Shao, X.H., Chen, S.T., Wu, J.Y., Jiang, X.Y., Wang, X.F., An, Z.S., 2008. Millennial- and orbital-scale changes in the East Asian monsoon over the past 224,000 years. Nature 451, 1090–1093.
- Xie, S.C., Evershed, R.P., Huang, X.Y., Zhu, Z.M., Pancost, R.D., Meyers, P.A., Gong, L.F., Hu, C.Y., Huang, J.H., Zhang, S.L., Gu, Y.S., Zhu, J.Y., 2013. Concordant monsoondriven postglacial hydrological changes in peat and stalagmite records and their impacts on prehistoric cultures in central China. Geology 41, 827–830.
- Yang, X.L., Liu, J.B., Liang, F.Y., Yuan, D.X., Yang, Y., Lu, Y.B., Chen, F.H., 2014. Holocene stalagmite δ^{18} O records in the East Asian monsoon region and their correlation with those in the Indian monsoon region. The Holocene 24, 1657–1664.
- Yin, J.J., Li, H.C., Rao, Z.G., Shen, C.-C., Mii, H.-S., Pillutla, R.K., Hu, H.-M., Li, Y.X., Feng, X.H., 2017. Variations of monsoonal rain and vegetation during the past millennium in Tiangui Mountain, North China reflected by stalagmite $\delta^{18}{\rm O}$ and $\delta^{13}{\rm C}$ records from Zhenzhu Cave. Quatern. Int. 447, 89–101.
- Zeng, G.N., Luo, W.J., Wang, S.J., Du, X.L., 2015. Hydrogeochemical and climatic interpretations of isotopic signals from precipitation to drip waters in Liangfeng Cave, Guizhou Province, China. Environ. Earth Sci. 74, 1509–1519.
- Zhang, H.B., Griffiths, M.L., Chiang, J.C.H., Kong, W.W., Wu, S.T., Atwood, A., Huang, J.H., Cheng, H., Ning, Y.F., Xie, S.C., 2018. East Asian hydroclimate modulated by the position of the westerlies during Termination I. Science 362, 580–583.
- Zhu, X.W., Wang, X.Y., Zhu, D.H., Gong, Z.Z., Qin, H.R., 1988. Study on Karst Geomorphology and Caves in Guilin. Geological Publishing House, Beijing, China, pp. 117–131 (in Chinese with English abstract).